ACS APPLIED NANO MATERIALS
Cite This: ACS Appl. Nano Mater. 2019, 2, 6629−6636
Article
www.acsanm.org

Porous Graphene Wrapped $SrTiO_3$ Nanocomposite: Sr−C Bond as an Effective Coadjutant for High Performance Photocatalytic Degradation of Methylene Blue

Harsha Bantawal,[†] Meenaketan Sethi,[†] U. Sandhya Shenoy,*[,‡] and D. Krishna Bhat*[,†]

[†]Department of Chemistry, National Institute of Technology Karnataka, Surathkal, Mangalore 575025, India
[‡]Department of Chemistry, College of Engineering and Technology, Srinivas University, Mukka, Mangalore 574146, India

Supporting Information

ABSTRACT: Porous graphene-$SrTiO_3$ (PGST) composite prepared by a facile solvothermal method was tested for its photocatalytic activity in degradation of methylene blue (MB) dye. First-principles density functional theory calculations were also carried out to study the effect of nanocomposite formation on the electronic structure and density of states. The combined experimental and theoretical study gave insights regarding the formation of the Sr−C bond which enhanced the charge transport, effectively separating the charge carriers and reduced their recombination rate. The formation of PGST nanocomposite favorably tuned the electronic structure with decreased band gap due to introduction of the hybridized states extending the absorption to the visible region of electromagnetic spectrum. The microscopy studies revealed loofah like PG wrapped $SrTiO_3$ nano structures with contusions providing high surface area facilitating adsorption of MB dye. Degradation of ∼92% was obtained by 7.5 PGST in 120 min with high cyclic stability indicating its suitability as an efficient photocatalyst for the treatment of pollutants.

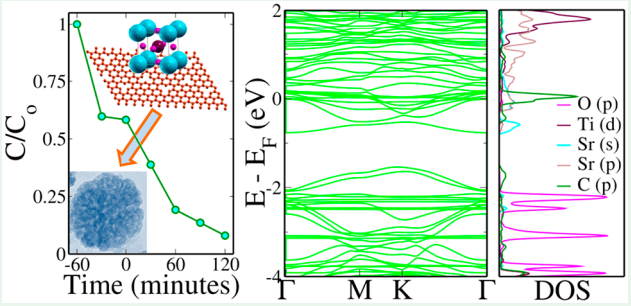

KEYWORDS: *porous graphene, $SrTiO_3$, photocatalysis, methylene blue, density functional theory, nanocomposite*

Downloaded via Sandhya Shenoy on October 29, 2019 at 09:27:01 (UTC).
See https://pubs.acs.org/sharingguidelines for options on how to legitimately share published articles.

1. INTRODUCTION

Photocatalysis constitutes the most propitious options for environmental remediation due to its efficient utilization of sunlight as a clean and renewable energy source.[1] In the last few decades, perovskite-oxide-based photocatalysts having general formula ABO_3 have been receiving attention due to their cost effectiveness, biocompatibility, and unique photocatalytic activity.[2] Among them, $SrTiO_3$ has attracted tremendous interest due to its very good physicochemical properties such as large number of active sites, excellent chemical and thermal stability, and environmentally benign nature.[3] However, it suffers from a major drawback as its photocatalytic activity is strictly restricted to the ultraviolet region of electromagnetic spectrum because of its wide band gap of 3.2 eV.[4] Although doping has been implemented to tune the electronic structure and reduce the band gap this leads to surfacing of another drawback viz. the high rate of recombination due to introduction of defect states of the dopant atom.[5,6] Also, poor transport of carriers leads to inefficient charge separation and hence reduced lifetime of photogenerated electron−hole pairs. Therefore, to facilitate the rapid transport of charge carriers to the reaction site blending $SrTiO_3$ with an efficient conducting material is essential.

Graphene, a 2D layer of sp^2 hybridized carbon atoms with a hexagonal motiff is known to possess high electrical conductivity, thermal conductivity, electron mobility, mechanical strength, and chemical stability.[7,8] Porous graphene (PG), on the other hand, possesses higher surface area, excellent hydrophobicity, higher stability, and acts as an electron acceptor.[9] Hence, $SrTiO_3$-PG composite is expected to exhibit high conductivity, adsorptivity, and enhanced photocatalytic activity. Although synthesis of $SrTiO_3$/graphene composites for photocatalytic applications has been previously reported, to the best of our knowledge synthesis of porous graphene-$SrTiO_3$(PGST) composite has not been reported.[10−12] Hence, development of a facile synthetic technique for producing highly efficient PGST composite for photocatalytic applications is highly anticipated. The goal is to design the synthesis such that the composite possesses high surface area, has appropriate band gap for visible light absorption, and the surface interaction between $SrTiO_3$ and PG is high so as to facilitate easy charge carrier transfer along with reduced tendency for recombination of photogenerated electron−hole pair.

Herein, PGST composite was prepared by a facile and reproducible one step solvothermal approach. The synthesized

Received: August 7, 2019
Accepted: September 18, 2019
Published: September 18, 2019

© 2019 American Chemical Society

DOI: 10.1021/acsanm.9b01513
ACS Appl. Nano Mater. 2019, 2, 6629−6636

Scheme 1. Schematic Illustration of Synthesis of PGST Composite via Solvothermal Method

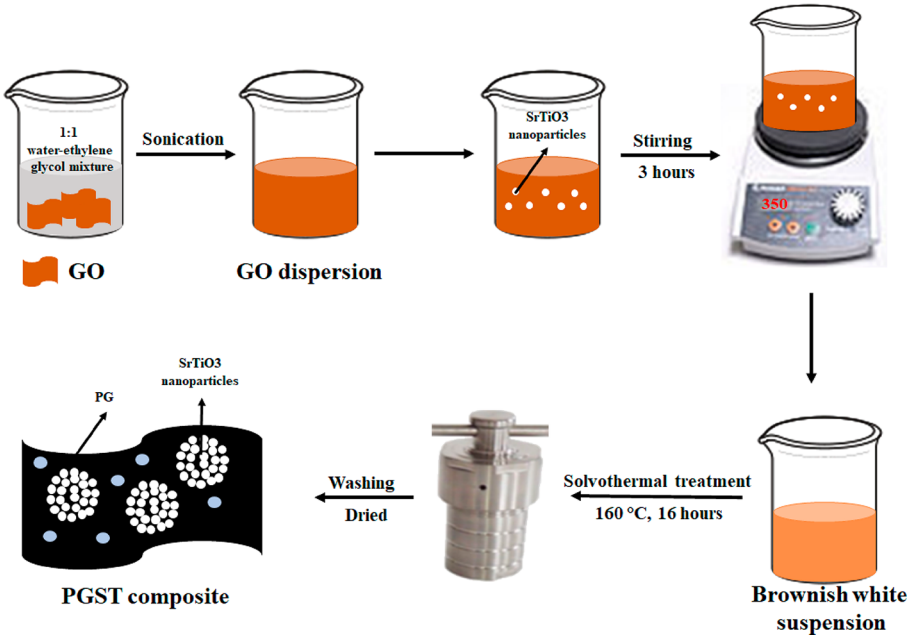

materials were thoroughly characterized by X-ray diffraction (XRD), Raman spectroscopy, X-ray photoelectron spectroscopy, field emission scanning electron microscopy (FESEM), transmission electron microscopy (TEM), Brunauer–Emmett–Teller (BET) analysis, diffuse reflectance (DR) spectroscopy, photoluminescence (PL) spectroscopy and electrochemical impedance spectroscopy (EIS) techniques. The photocatalytic efficiency of PGST was assessed by analyzing the degradation of methylene blue (MB) dye solution. Meanwhile, density functional theory (DFT) calculations of PGST were carried out to understand the perturbation of the electronic structure due to composite formation. The superior photocatalytic activity of the composite was mainly attributed to the high adsorption ability due to large surface area, visible light absorption due to reduced band gap and low recombination rate of photogenerated charges due to increased rate of charge transfer as a consequence of Sr–C bond formation in the composite.

2. METHODS

2.1. Synthesis of PGST Composite. All chemicals were procured from Sigma-Aldrich and were used without further purification. GO, PG, and $SrTiO_3$ were synthesized according to previously reported procedure.[9,13] "*x* PGST" (*x* = 2.5, 5.0, 7.5, and 10.0 wt % GO) was synthesized by a simple solvothermal approach (Scheme 1). A calculated amount of $SrTiO_3$ powder was added to the solution of GO dispersed in 1:1 water–ethylene glycol mixture and stirred for 3 h to obtain a homogeneous solution. The resultant mixture was sealed in an autoclave and then heated to 160 °C for 16 h. The obtained black precipitates were thoroughly washed with distilled water and dried in an oven at 70 °C for 8 h. The composite obtained by taking 2.5, 5.0, 7.5, and 10.0 wt % GO was labeled as 2.5 PGST, 5.0 PGST, 7.5 PGST, and 10 PGST, respectively.

2.2. Characterization. The crystallographic structures of the as synthesized catalysts were analyzed using a powder X-ray diffractometer (XRD, Rigaku Miniflex 600) with monochromatic Cu–K_α radiation (λ = 0.154 nm) at a scan rate of 2° per min in the range of 5–80°. Raman spectra were recorded with the help of a He–Ne source operating at 532 nm (Renishaw Invia). Kratos XSAM800 spectrometer equipped with an Al K_α source was used to record X-ray photoelectron spectrum (XPS). The morphological features of the synthesized catalysts were analyzed using field emission scanning electron microscope (FESEM, Carl Zeiss Ultra 55) and transmission electron microscope (TEM, Fie Tecnai G2). The nitrogen adsorption–desorption isotherms were obtained at 77 K using BEL SORP II, JAPAN. The specific surface areas of the as synthesized catalysts were calculated by BET method and the Barrett–Joyner–Halenda (BJH) method was employed to determine pore size distribution.[14] DR spectrum was taken using UV–visible DR spectrometer (DRS, DR SPECORD S600 Analytic Jena) and the PL spectra were obtained with a 288 nm excitation wavelength source (LS-55, PerkinElmer Instruments) at room temperature. EIS was carried out in the frequency range of 10^5 Hz to 0.01 Hz by applying a small AC perturbation of 10 mV using a three-electrode cell with composite coated Ni sheet as working electrode, Pt wire as counter electrode and saturated calomel electrode as reference electrode with 6 M KOH as electrolyte using IVIUM electrochemical workstation (The Netherlands, Vertex).[14] The working electrode was fabricated according to a previously reported paper.[9]

2.3. Determination of Photocatalytic Activity. The photocatalytic reactor was fitted with a high-pressure 250 W Hg vapor lamp functioning at a wavelength of 410–700 nm. PGST (25 mg) and MB (1 mg) dissolved in 100 mL of water were loaded into a 500 mL of pyrex glass beaker. Adsorption–desorption equilibrium was attained by magnetic stirring for 1 h. In these studies, 5 mL of the MB solution was drawn out periodically, centrifuged to remove the catalyst and the absorbance of the dye solution was measured using UV–visible spectrometer at 664 nm. The percentage of degradation of dye was calculated as per eq 1.[15]

$$\%\text{degradation} = [(C_o - C)/C_o] \times 100 \quad (1)$$

where, C_o is the concentration of dye solution at time, t = 0 and C is the concentration at different time intervals.

2.4. Computational Details. To understand the mechanism of photocatalytic activity of PGST, DFT based electronic structure calculations were carried out using Quantum ESPRESSO package.[16] Ionic core and valence electrons were represented using plane wave basis set and ultrasoft pseudopotentials. Generalized gradient approximation with Perdew, Burke, and Erzenhoff parametrized form is used to treat the exchange-correlation energy functional.[17] $5s^2$, $3d^24s^2$, $2s^22p^4$, $2s^22p^2$ electrons of Sr, Ti, O, and C, respectively are considered as valence electrons in the calculations. Fully relaxed 5 × 5 × 1 supercell of PG along with $SrTiO_3$ cluster was used for simulating

DOI: 10.1021/acsanm.9b01513
ACS Appl. Nano Mater. 2019, 2, 6629–6636

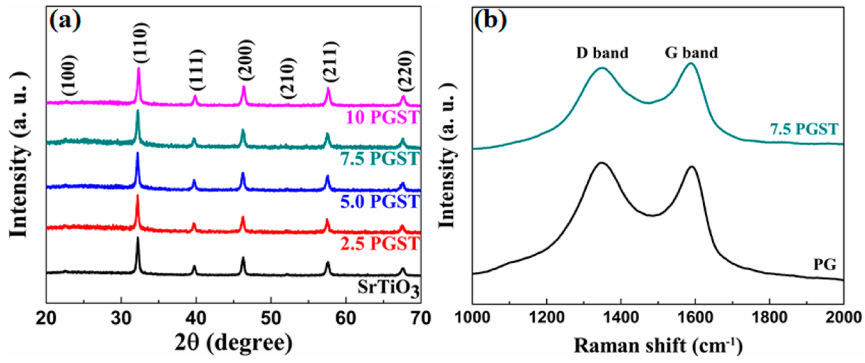

Figure 1. (a) XRD patterns of $SrTiO_3$ and PGST samples; (b) Raman spectra of PG and 7.5 PGST.

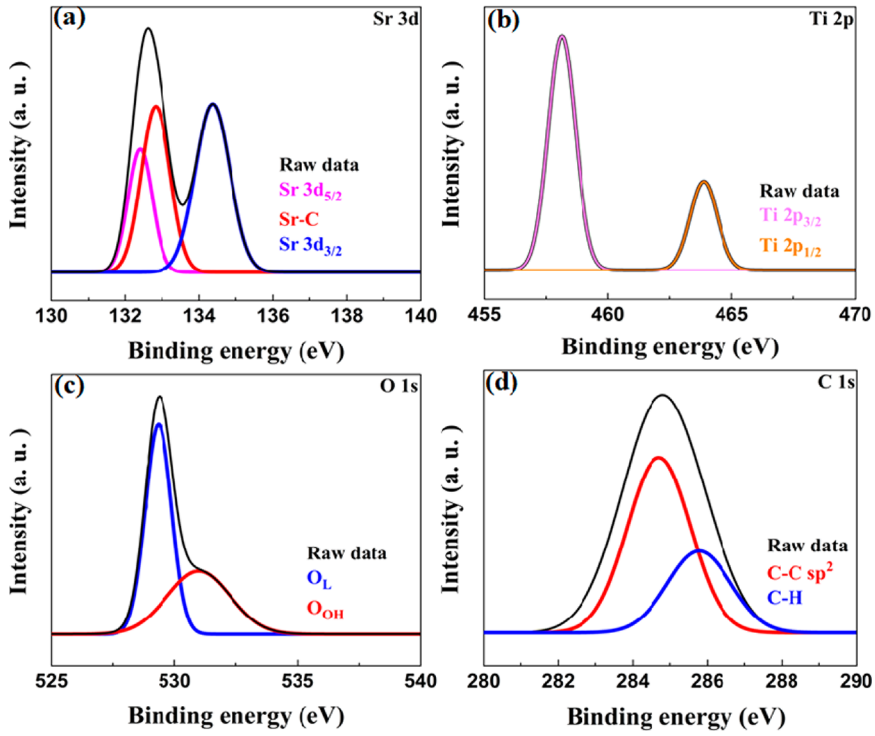

Figure 2. High resolution XPS spectrum of 7.5 PGST (a) Sr 3d; (b) Ti 2p; (c) O 1s; (d) C 1s.

the composite. A vacuum of 12 Å was used in the z - direction to avoid the interaction between the successive layers. Brillouin zone was sampled using a k mesh of 9 × 9 × 1 for self-consistent field calculations and 18 × 18 × 1 for nonself consistent field calculations. An energy cutoff of 50 Ry for plane wave basis and charge density cutoff of 400 Ry was used. Electronic structure was determined along Γ - M - K - Γ path of high symmetry points for the composite.

3. RESULTS AND DISCUSSION

3.1. XRD and Raman Analysis. XRD technique was used for the crystallographic study of the as synthesized catalysts. The peak indexed XRD plot (Figure 1a) of PGST samples matches well with the cubic phase of $SrTiO_3$ (JCPDS card no. 01−089−4934). A small shift in the 2θ value of (110) peak from 32.21° ($SrTiO_3$) to 32.17° (7.5 PGST) indicates the possible interaction between the components of the composite formed. Scherrer equation was used to calculate the average crystal sizes using (110) peak. The calculated values turned out to be 34.7, 32.8, 30.0, 28.8, and 26.1 nm for $SrTiO_3$, 2.5 PGST, 5.0 PGST, 7.5 PGST, and 10 PGST, respectively. Due to lower quantity of PG in the composite, peaks corresponding to it are absent. However, its presence is confirmed from Raman spectra. Among the different composite samples, 7.5 PGST showed highest photocatalytic activity. Hence, for detailed analysis, only 7.5 PGST sample was considered.

The Raman spectra of PG reveals a peak at 1347.5 cm^{-1} (D band), which can be assigned to the presence of sp^3 defects and another peak at 1590.7 cm^{-1}(G band), which can be attributed to the in-plane vibration of sp^2 bonded carbon atoms (Figure 1b).[9] These peaks shift to 1348.8 and 1588.5 cm^{-1}, respectively in 7.5 PGST. It is seen that the intensity ratio of D band to G band (I_D/I_G) in the case of 7.5 PGST (0.94) is lower than that of PG (1.05). This is attributed to the interaction of PG with $SrTiO_3$ moiety which neutralizes the free defects present in the PG.[7]

3.2. XPS Analysis. XPS survey spectrum of 7.5 PGST reveals the presence of Sr, Ti, O, and C (SI Figure S1). The peaks at binding energies 132.5 and 134.3 eV is attributed to Sr $3d_{5/2}$ and Sr $3d_{3/2}$ states, respectively (Figure 2a).[13] While, the peak at 132.96 corresponds to Sr bonded to C. This suggests the chemical interaction of $SrTiO_3$ with the PG in the

DOI: 10.1021/acsanm.9b01513
ACS Appl. Nano Mater. 2019, 2, 6629−6636

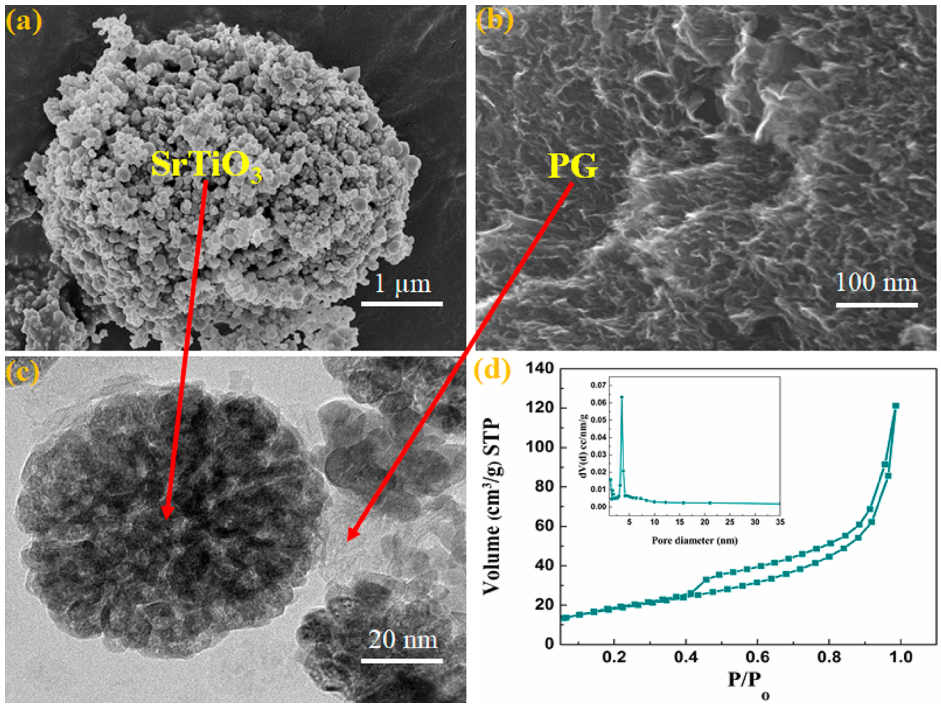

Figure 3. FESEM image of (a) $SrTiO_3$ nanoparticles; (b) PG; (c) TEM image of 7.5 PGST; (d) Nitrogen adsorption−desorption isotherm and BJH pore size distribution (inset) of 7.5 PGST.

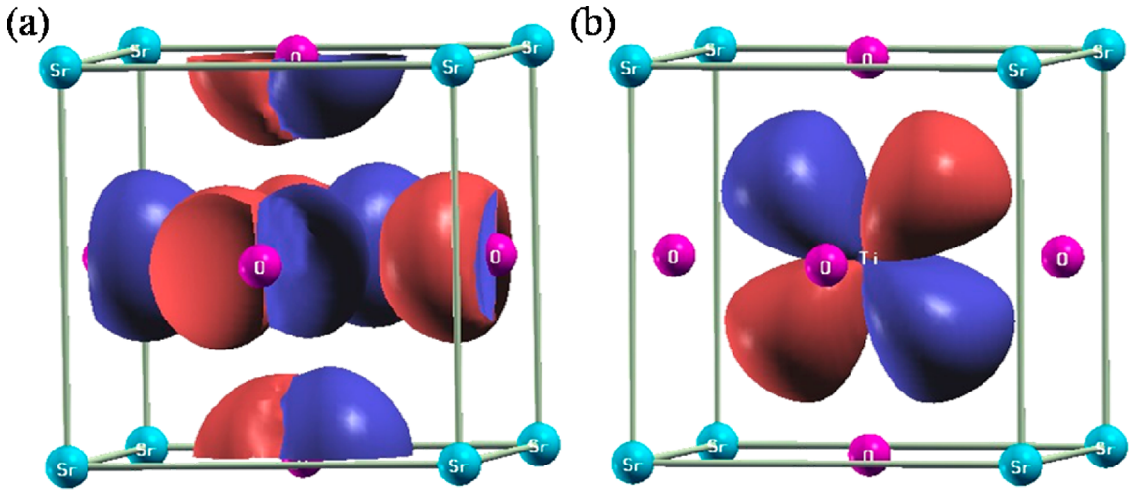

Figure 4. Visualization of wave functions of $SrTiO_3$ of (a) valence band; (b) conduction band.

composite which is favorable for transport of photogenerated electrons. One of the main reasons of low efficiency of a photocatalyst despite having a favorable band gap is the recombination of charge carriers. Formation of Sr−C bonds facilitates the transfer of electrons generated in $SrTiO_3$ to electron accepting PG, there by separating the electrons and holes and reducing the recombination of the charges. This is further confirmed by the DFT studies. Ti $2p_{3/2}$ and Ti $2p_{1/2}$ states appear as peaks in Figure 2b at binding energies of 458.13 and 463.93 eV, respectively.[13] The peak at 529.3 eV in Figure 2c is due to the lattice oxygen (O_L) and at 531.2 eV is due to the surface hydroxyl groups (O_{OH}).[13] Figure 2d shows the high resolution C 1s spectrum which is deconvoluted into two peaks of binding energies 284.7 and 285.7 eV and is attributed to sp^2 carbon of PG and C−H bond of sp^3 carbon atom at the edge of PG, respectively.[9]

3.3. Morphology Studies and Surface Area Analysis.

The morphological study of 7.5 PGST was carried out using FESEM and TEM. Figure 3a reveals $SrTiO_3$ nanoparticles as spherical agglomerates, whereas Figure 3b shows PG in the form of wrinkled sheets with porous nature. The TEM image of 7.5 PGST shows $SrTiO_3$ nanoparticles being wrapped in PG sheets and the entire composite having a loofah like structure (Figure 3c). The wrapping of nanoparticles by PG increases the area of contact between the two components facilitating better interaction for charge transfer in comparison to $SrTiO_3$ particles being just distributed on the planar PG sheets.[9,10] The SAED pattern of 7.5 PGST shows polycrystalline nature (SI Figure S2).

The nitrogen adsorption analysis was carried out in order to obtain the information on the specific surface area and porosity of PGST. The isotherms for 7.5 PGST was type IV with

DOI: 10.1021/acsanm.9b01513
ACS Appl. Nano Mater. 2019, 2, 6629−6636

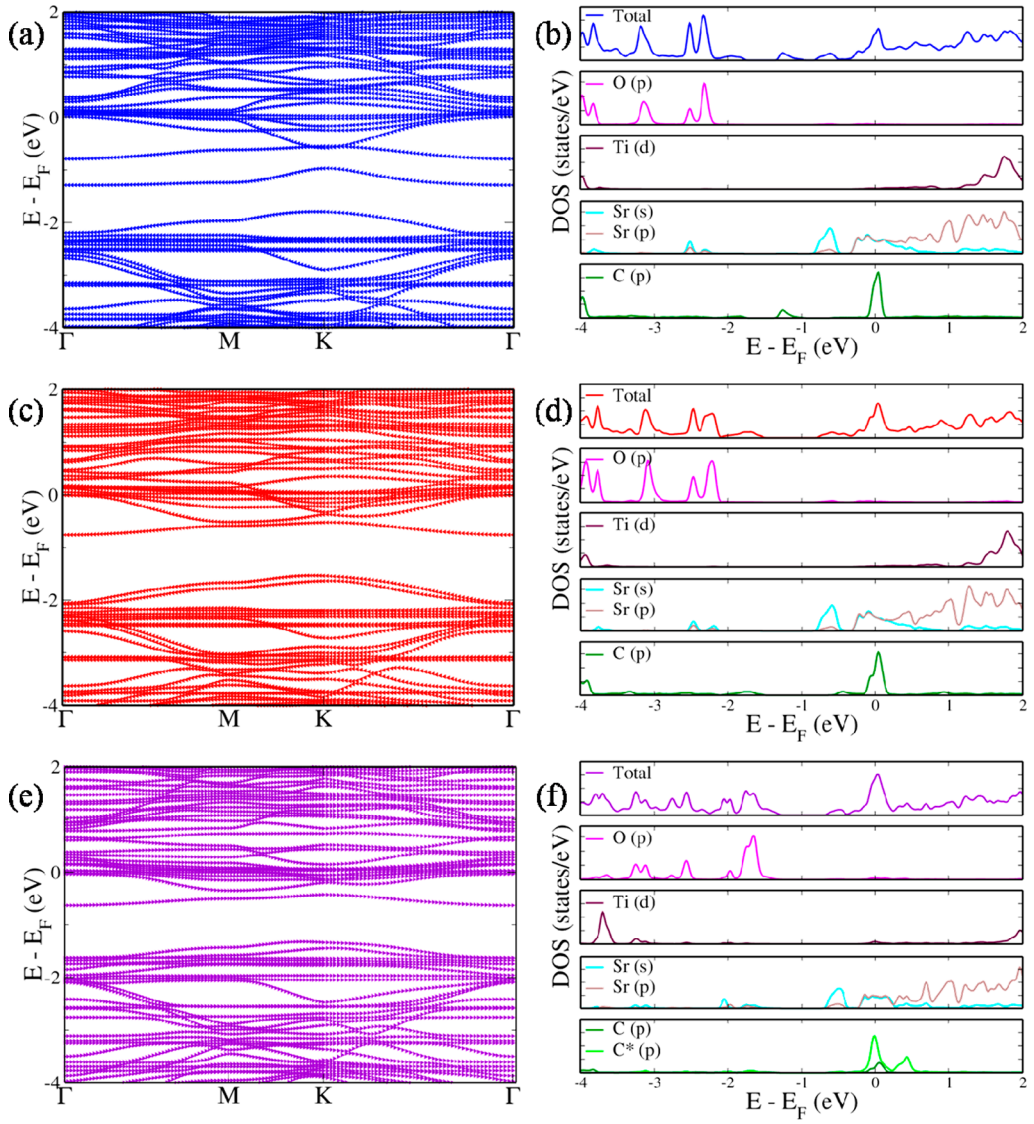

Figure 5. Electronic structure and pdos of (a) and (b) C−I; (c) and (d) C−II; (e) and (f) D-I. Energy is shifted with respect to Fermi level which is set at zero.

hysteresis loops of type H3, indicating the presence of slit like pores (Figure 3d).[18] The BET specific surface area of 7.5 PGST was found to be 65.35 m^2g^{-1}, which is much greater than $SrTiO_3$ (26.45 m^2g^{-1}). The large surface area of the composite is due to the formation of contusions in the loofah like structure. This in turn allows more MB dye molecules to get adsorbed on to the surface of the catalyst due to the $\pi-\pi$ interaction between the PG and MB dye molecule. The photogenerated carrier migrates to the surface of the material to react with oxygen or water to form active species. Adsorption of MB dye on the surface of catalyst decreases the path length to be traveled by the active species for the effective reaction and hence increases the photocatalytic activity. The Barrett−Joyner−Halenda (BJH) method was utilized to analyze the pore size distribution of 7.5 PGST indicating the presence of mesopores with the pore volume of 0.151 cm^3g^{-1} (Figure 3d inset) while that of $SrTiO_3$ was 0.040 cm^3g^{-1}. The pore size distribution of $SrTiO_3$ is given in SI Figure S3.

3.4. Electronic Structure Analysis. The electronic structure of $SrTiO_3$ is composed of O 'p' states constituting the valence band (VB) and Ti 'd' states constituting the conduction band (CB) as revealed by the visualization of its wave functions (Figure 4). A direct band gap (Γ point) of 2.74 eV and an indirect band gap (R → Γ) of 2.14 eV is estimated from DFT calculations against the experimental band gap of 3.2 eV due to the well-known underestimation in DFT based calculations.[4] Graphene is known to possess a zero band gap at K point while PG has a gap of ∼1.4 eV between VB and CB with an asymmetric defect band of ∼0.4 eV width (passing in the mid gap region) arising out of 'p' states of C atom surrounding the pore.[9]

In order to study the electronic structure of PGST, two different conditions were considered. In condition C−I, PG containing a single pore within the simulated area (5 × 5 × 1 supercell) was chosen. As in the case of pristine $SrTiO_3$, even here VB is formed to a major extent out of O 'p' orbital contribution while CB out of Ti 'd' orbitals. A prominent decrease in the band gap to 1.21 eV is seen with the introduction of levels comprising of 'p' states of C atoms about 0.82 eV above the VB edge. The presence of these in-gap states extends the absorption into the visible range. In addition to

DOI: 10.1021/acsanm.9b01513
ACS Appl. Nano Mater. 2019, 2, 6629−6636

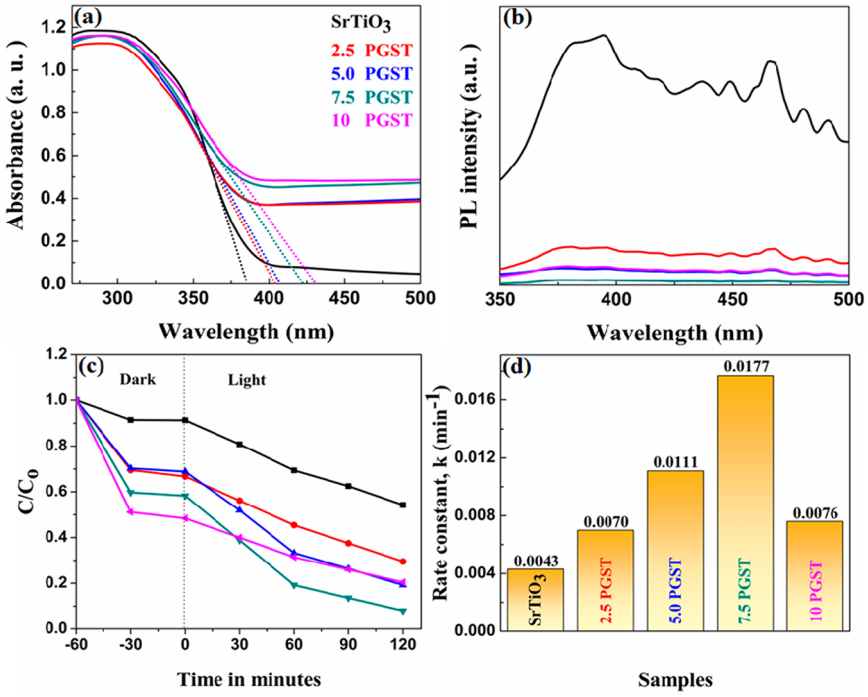

Figure 6. (a) UV−visible DR spectra; (b) PL spectra; (c) Kinetics of photocatalytic degradation; (d) Rate constants of the photocatalytic degradation of MB by the synthesized $SrTiO_3$ and PGST.

this 's' states of Sr atoms along with minor contribution of its 'p' orbitals form a level just beneath the CB overlapping with the CB edge at K point (Figure 5a and b). A noteworthy observation here is that the occurrence of this level due to Sr atoms is quite a unique feature as in general, Sr states never contribute in and around the Fermi level in $SrTiO_3$ based materials.[4,19] At the Fermi level the 'p' orbitals of C hybridize with 's' and 'p' orbitals of Sr leading to a peak in the DOS plot. The above two features point toward the formation of Sr−C chemical bond between the $SrTiO_3$ and PG confirming the results of XPS. The formation of Sr−C bond facilitates easier migration of charge carriers and hence lesser instances of recombination of photo induced electron hole pairs. To mimic higher porosity, two pores were considered in the same supercell (5 × 5 × 1) viz. the condition, C−II. The electronic structure and DOS of C−II reveals that the C induced mid gap states found in C−I is pushed further down and overlaps with the VB. This increases the gap from C defect band to CB to 1.02 eV from 0.39 eV (estimated in the case of C−I) and indicates lesser chances of recombination (Figure 5c and d). The other features of the electronic structure of C−II resemble that of C−I. The absence of mid gap level in C−II and formation of stronger Sr−C bond due to higher extent of overlap of C and Sr orbitals indicates that increase in the number of pores not only increases the surface area for adsorption of substrate but also improves the photocatalytic activity by facilitating better charge migration and hence better charge separation. Since there is a possibility of C being doped into the $SrTiO_3$ lattice during the synthesis of PGST, we studied two different types of doped composites, viz. C@Sr site (D-I) and C@Ti site (D-II) with two pores in the PG supercell. The electronic structure of D-I reveals that at the Fermi level the states are contributed majorly by the 'p' orbital of C@Sr site with minor contributions from each C atom of PG sheet. Since the doped C atom bonds with the O atom of the lattice, their orbitals hybridize, and the contribution of O 'p' orbitals move further up in the VB toward the Fermi level reducing the band gap to 0.97 eV (Figure 5e and f). This appears as a stripe just beneath the curved edge of VB. The Sr states appear just 0.08 eV below the CB, 10 times lower than that in the undoped case (C-II). The D-II configuration reveals a further decrease in the band gap to 0.84 eV. Unlike the other three configurations here, overlap of orbitals of Sr with C or of Ti with C is not observed. The 'p' orbitals of C@Ti shows major contributions in the VB (2.5 eV below Fermi level) and at the top of CB away from Fermi level unlike C@Sr which had its effect exactly at the Fermi level (SI Figure S4). The 'p' orbitals of C atoms of PG form the lowermost part of the CB. Interestingly, Ti 's' states form a donor level 0.21 eV above the VB but 0.38 eV below the Fermi level within the band gap region of 0.84 eV. Around 0.5 eV above the Fermi level in the CB contributions from both 'd' states of Ti and 's' states of Sr is observed. In total, the simulated electronic structure and DOS of PGST reveals a decrease in band gap extending the absorption to visible range and the formation of Sr−C bond which helps in transfer of electrons from $SrTiO_3$ to PG facilitating charge separation and hence reduced recombination of electron and holes enhancing the photocatalytic activity as experimentally observed.

3.5. Optical, Electrochemical, and Photocatalytic Study. The UV-visible absorbance plot of $SrTiO_3$ exhibited an absorption edge at 387 nm, due to the electronic transition from the O 'p' to the Ti 'd' states. The absorption band edges of PGST exhibited a red shift from 405 to 431 nm (Figure 6a). The Tauc relation was employed to calculate the direct band gap of the as synthesized samples as given in eq 2.[20]

$$(a\mathrm{h}\nu)^2 = \mathrm{K}(h\nu - E_g) \quad (2)$$

where, a is the absorption coefficient, E_g is the energy band gap of the semiconductor, K is a constant, hν is the energy of

DOI: 10.1021/acsanm.9b01513
ACS Appl. Nano Mater. 2019, 2, 6629−6636

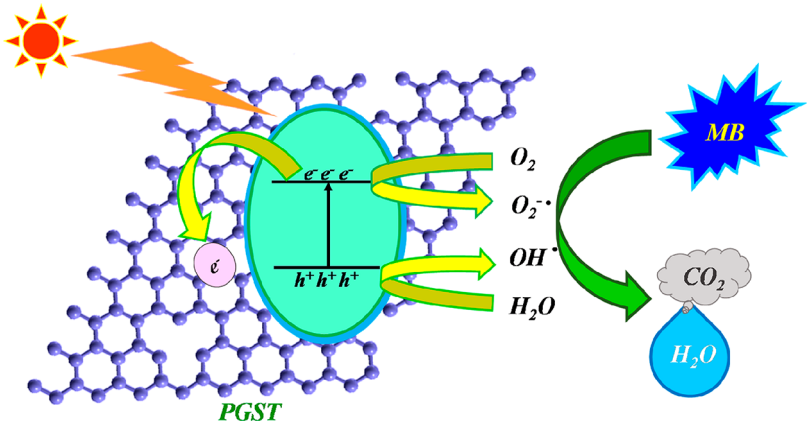

Figure 7. Mechanism of photocatalytic degradation of MB by PGST.

photon. $SrTiO_3$ exhibited a band gap of 3.21 eV, whereas the band gap (aborption edge) of the PGST samples decreased gradually from 3.06 eV (405 nm), 3.03 eV (409 nm), 2.93 eV (424 nm) to 2.87 eV (431 nm) for 2.5 PGST, 5 PGST, 7.5 PGST, and 10 PGST, respectively. This decrease in the band gap of PGST is attributed to the formation of C 'p' states above the VB and Sr 's' states below the CB as explained in detail in previous section under the DFT studies.

The PL spectra of the as synthesized $SrTiO_3$ and PGST were examined in order to get more information on recombination behavior of photoinduced charges (Figure 6b). Compared with $SrTiO_3$, a severe decrease in the fluorescence intensity of PGST samples can be observed. This decrease in the PL intensity of the PGST samples is because of the lower recombination rate of photoinduced holes and electrons due to efficient electron transfer from $SrTiO_3$ by the PG through Sr−C bond. Further increasing the PG content above its optimal value resulted in the enhancement of fluorescence intensity due to agglomeration of PG which again introduces recombination centers.

Nyquist plot showed that the addition of PG decreased the resistance value of $SrTiO_3$ from 3.18 Ω to 0.19 Ω for 7.5 PGST (SI Figure S5). Although the values decreased with the increase in amount of PG, the 10 PGST sample showed comparatively higher resistance which may be due to the agglomeration of PG sheets. Further, the obtained resistance values from EIS measurements revealed that combination of $SrTiO_3$ with PG decreases the interfacial as well as charge transfer resistance (SI Table S1). This leads to decrease in the recombination of photogenerated charge carriers due to the increased rate of electron acceptance and transport by PG.[21]

The percentage degradation of MB by $SrTiO_3$, 2.5 PGST, 5.0 PGST, 7.5 PGST, and 10 PGST was found to be 45.7, 70.4, 80.8, 91.9, and 79.5, respectively (Figure 6c). The enhanced photocatalytic activity of 7.5 PGST can be attributed to the enhanced light absorption in the visible region, high surface area, high pore volume and low recombination rate of photoinduced charges. Large surface area of the 7.5 PGST composite allows more MB dye molecules to get adsorbed on to the surface of the catalyst and the higher pore volume leads to rapid diffusion of various inorganic products formed during the photocatalytic reaction.[21] On the other hand, in the case of 10 PGST, the higher amount of PG content hinders the absorption of light by $SrTiO_3$ nanoparticles which can cause decreased generation of electron−hole pair.[7] The presence of excess PG can also act as recombination center for photo-induced electron−hole pairs as revealed by PL results. Due to these reasons, the photocatalytic activity of 10 PGST was found to be lower. The above photocatalytic reaction follows the pseudo first-order rate eq 3.[22]

$$\ln(C/C_o) = -kt \tag{3}$$

where, C_o is the concentration of the dye at time $t = 0$, C is the concentration of the dye at irradiation time 't' and k is the first order rate constant (Figure 6d). It is found that the rate constant increases with increase in PG content. 7.5 PGST exhibited a value of 0.0177 min^{-1}, which is higher than the $SrTiO_3$ (0.0043 min^{-1}). The drop in the photocatalytic activity of 7.5 PGST after five consecutive cycles was minimal, pointing to its high stability (SI Figure S6).

In order to find out the active species involved in the photocatalytic degradation, trapping experiments were carried out using different agents such as benzoquinone (1 mM) as a superoxide anion radical ($O_2^{-}\cdot$) scavenger, potassium iodide (10 mM) as a hole (h^+) scavenger and isopropyl alcohol (10 mM) as a hydroxyl radical (OH·) scavenger. The addition of potassium iodide reduced the photocatalytic activity to the maximum extent followed by isopropyl alcohol indicating holes and hydroxyl radicals are the major active species (SI Figure S7). Benzoquinone addition had the least effect indicating $O_2^{-}\cdot$ had minor role in the degradation of MB. Taking into consideration of these results, the mechanism of photocatalytic degradation of MB by PGST can be explained as follows (Figure 7). When a photon of suitable energy is irradiated on PGST, electron hole pairs are generated in $SrTiO_3$. As PG is an electron acceptor, the electrons from the $SrTiO_3$ transfers to it through the Sr−C bond thereby reducing the rate of recombination of photoinduced charges and boost the photocatalytic activity. These electrons react with oxygen to produce superoxide radicals and the holes either directly oxidize MB or react with surface adsorbed water to produce hydroxyl radicals. These generated active species act as strong oxidizer for the effectual degradation of the MB adsorbed on the PGST to CO_2 and H_2O.

4. CONCLUSIONS

For the first time, a facile solvothermal method was successfully used for the synthesis of PGST. The loofah like structures of the composite increased the surface area facilitating higher rate of adsorption of MB dye. First-principles DFT simulations revealed a reduction in the band gap of $SrTiO_3$ on integration with PG, extending the absorption to

DOI: 10.1021/acsanm.9b01513
ACS Appl. Nano Mater. 2019, 2, 6629−6636

the visible region of the spectrum. The increased rate of charge transfer due to the formation of Sr−C bond, enhanced the charge separation, and reduced the recombination rate. The composite exhibited enhanced photocatalytic activity (∼92% in 120 min) and cyclic stability. The high performance of the PGST is attributed to the tuned electronic structure, morphology, and chemical bonding, which makes it a potential candidate for photocatalytic environmental remediation.

■ ASSOCIATED CONTENT

Supporting Information

The Supporting Information is available free of charge on the ACS Publications website at DOI: 10.1021/acsanm.9b01513.

XPS survey spectrum, SAED pattern, pore size distribution of $SrTiO_3$, electronic structure and pdos of D-II, Nyquist plot, resistance and conductance values, reusability test, scavenger test (PDF)

■ AUTHOR INFORMATION

Corresponding Authors

*(U.S.S.) E-mail: sandhyashenoy347@gmail.com.
*(D.K.B.) E-mail: denthajekb@gmail.com.

ORCID

U. Sandhya Shenoy: 0000-0002-6786-882X
D. Krishna Bhat: 0000-0003-0383-6017

Notes

The authors declare no competing financial interest.

■ REFERENCES

(1) Yang, X.; Wang, D. Photocatalysis: From Fundamental Principles to Materials and Applications. *ACS Appl. Energy Mater.* **2018**, *1*, 6657−6693.

(2) Moniruddin, M.; Ilyassov, B.; Zhao, X.; Smith, E.; Serikov, T.; Ibrayev, N.; Asmatulu, R.; Nuraje, N. Recent Progress on Perovskite Materials in Photovoltaic and Water Splitting Applications. *Mater. Today Energy* **2018**, *7*, 246−259.

(3) Phoon, B. L.; Lai, C. W.; Juan, J. C.; Show, P. L.; Chen, W. H. A Review of Synthesis and Morphology of $SrTiO_3$ for Energy and Other Applications. *Int. J. Energy Res.* **2019**, *435151*.

(4) Bantawal, H.; Shenoy, U. S.; Bhat, D. K. Tuning the Photocatalytic Activity of $SrTiO_3$ by Varying the Sr/Ti Ratio: Unusual Effect of Viscosity of the Synthesis Medium. *J. Phys. Chem. C* **2018**, *122*, 20027−20033.

(5) Kawasaki, S.; Akagi, K.; Nakatsuji, K.; Yamamoto, S.; Matsuda, I.; Harada, Y.; Yoshinobu, J.; Komori, F.; Takahashi, R.; Lippmaa, M.; Sakai, C. Elucidation of Rh-induced In-gap States of Rh: $SrTiO_3$ Visible-Light-Driven Photocatalyst by Soft X-ray Spectroscopy and First-Principles Calculations. *J. Phys. Chem. C* **2012**, *116*, 24445−24448.

(6) Kawasaki, S.; Takahashi, R.; Akagi, K.; Yoshinobu, J.; Komori, F.; Horiba, K.; Kumigashira, H.; Iwashina, K.; Kudo, A.; Lippmaa, M. Electronic Structure and Photoelectrochemical Properties of an Ir-doped $SrTiO_3$ Photocatalyst. *J. Phys. Chem. C* **2014**, *118*, 20222−20228.

(7) Sadiq, M. M. J.; Shenoy, U. S.; Bhat, D. K. Novel RGO−$ZnWO_4$−Fe_3O_4Nanocomposite as High Performance Visible Light Photocatalyst. *RSC Adv.* **2016**, *6*, 61821−61829.

(8) Mohamed, M. J. S.; Shenoy, U. S.; Bhat, D. K. High Performance Dual Catalytic Activity of Novel Zinc Tungstate-Reduced Graphene Oxide Nanocomposites. *Adv. Sci., Eng. Med.* **2017**, *9*, 115−121.

(9) Sethi, M.; Bantawal, H.; Shenoy, U. S.; Bhat, D. K. Eco-Friendly Synthesis of Porous Graphene and its Utilization as High Performance Supercapacitor Electrode Material. *J. Alloys Compd.* **2019**, *799*, 256−266.

(10) He, C.; Bu, X.; Yang, S.; He, P.; Ding, G.; Xie, X. Core-Shell $SrTiO_3$/Graphene Structure by Chemical Vapor Deposition for Enhanced Photocatalytic Performance. *Appl. Surf. Sci.* **2018**, *436*, 373−381.

(11) Ahmadi, M.; Dorraji, M. S.; Rasoulifard, M. H.; Amani-Ghadim, A. R. The Effective Role of Reduced-Graphene Oxide in Visible Light Photocatalytic Activity of Wide Band Gap $SrTiO_3$ Semiconductor. *Sep. Purif. Technol.* **2019**, *228*, 115771.

(12) Govindasamy, M.; Wang, S. F.; Pan, W. C.; Subramanian, B.; Ramalingam, R. J.; Al-Lohedan, H. Facile Sonochemical Synthesis of Perovskite-Type $SrTiO_3$ Nanocubes with Reduced Graphene Oxide Nanocatalyst for an Enhanced Electrochemical Detection of α-Amino Acid (Tryptophan). *Ultrason. Sonochem.* **2019**, *56*, 193−199.

(13) Shenoy, U. S.; Bantawal, H.; Bhat, D. K. Band Engineering of $SrTiO_3$: Effect of Synthetic Technique and Site Occupancy of Doped Rhodium. *J. Phys. Chem. C* **2018**, *122*, 27567−27574.

(14) Sethi, M.; Bhat, D. K. Facile Solvothermal Synthesis and High Supercapacitor Performance of $NiCo_2O_4$ Nanorods. *J. Alloys Compd.* **2019**, *781*, 1013−1020.

(15) Sadiq, M. M. J.; Shenoy, S. U.; Bhat, D. K. Novel NRGO-$CoWO_4$-Fe_2O_3Nanocomposite as an Efficient Catalyst for Dye Degradation and Reduction of 4-Nitrophenol. *Mater. Chem. Phys.* **2018**, *208*, 112−122.

(16) Giannozzi, P.; Baroni, S.; Bonini, N.; Calandra, M.; Car, R.; Cavazzoni, C.; Ceresoli, D.; Chiarotti, G. L.; Cococcioni, M.; Dabo, I.; Corso, A. L.; de Gironcoli, S.; Fabris, S.; Fratesi, G.; Gebauer, R.; Gerstmann, U.; Gougoussis, C.; Kokalj, A.; Lazzeri, M.; Martin-Samos, L.; Marzari, N.; Mauri, F.; Mazzarello, R.; Paolini, S.; Pasquarello, A.; Paulatto, L.; Sbraccia, C.; Scandolo, S.; Sclauzero, G.; Seitsonen, A. P.; Smogunov, A.; Umari, P.; Wentzcovitch, R. M. Quantum ESPRESSO: A Modular and Open-Source Software Project for Quantum Simulations of Materials. *J. Phys.: Condens. Matter* **2009**, *21*, 395502.

(17) Perdew, J. P.; Burke, K.; Ernzerhof, M. Generalized Gradient Approximation Made Simple. *Phys. Rev. Lett.* **1996**, *77*, 3865−3868.

(18) Sadiq, M. M. J.; Shenoy, S. U.; Bhat, D. K. $NiWO_4$-ZnO-NRGO Ternary Nanocomposite as an Efficient Photocatalyst for Degradation of Methylene Blue and Reduction of 4-Nitro Phenol. *J. Phys. Chem. Solids* **2017**, *109*, 124−133.

(19) Chen, H. C.; Huang, C. W.; Wu, J. C.; Lin, S. T. Theoretical Investigation of the Metal-Doped $SrTiO_3$ Photocatalysts for Water Splitting. *J. Phys. Chem. C* **2012**, *116*, 7897−7903.

(20) Sadiq, M. M. J.; Shenoy, U. S.; Bhat, D. K. Synthesis of $BaWO_4$/NRGO−gC_3N_4Nanocomposites with Excellent Multifunctional Catalytic Performance via Microwave Approach. *Front. Mater. Sci.* **2018**, *12*, 247−263.

(21) Kampouri, S.; Stylianou, K. C. Dual-Functional Photocatalysis for Simultaneous Hydrogen Production and Oxidation of Organic Substances. *ACS Catal.* **2019**, *9*, 4247−4270.

(22) Sadiq, M. M. J.; Shenoy, U. S.; Bhat, D. K. Enhanced Photocatalytic Performance of N-Doped RGO-$FeWO_4$/Fe_3O_4 Ternary Nanocomposite in Environmental Applications. *Mater. Today Chem.* **2017**, *4*, 133−141.

DOI: 10.1021/acsanm.9b01513
ACS Appl. Nano Mater. 2019, 2, 6629−6636